

Minimization of magnetic forces on Stellarator coils

Rémi Robin^{*}, ¹ and Francesco Volpe ^{†2}

¹Laboratoire Jacques-Louis Lions, Sorbonne Université
²Renaissance Fusion, <https://stellarator.energy>

March 25, 2021

Abstract

Magnetic confinement devices for nuclear fusion can be large and expensive. Compact stellarators are promising candidates for cost-reduction, but introduce new difficulties: confinement in smaller volumes requires higher magnetic field, which calls for higher coil-currents and ultimately causes higher Laplace forces on the coils - if everything else remains the same. This motivates the inclusion of force reduction in stellarator coil optimization. In the present paper we consider a coil winding surface, we prove that there is a natural and rigorous way to define the Laplace force (despite the magnetic field discontinuity across the current-sheet), we provide examples of cost associated (peak force, surface-integral of the force squared) and discuss easy generalizations to parallel and normal force-components, as these will be subject to different engineering constraints. Such costs can then be easily added to the figure of merit in any multi-objective stellarator coil optimization code. We demonstrate this for a generalization of the REGCOIL code [1], which we rewrote in python, and provide numerical examples for the NCSX (now QUASAR) design. We present results for various definitions of the cost function, including peak force reductions by up to 40 %, and outline future work for further reduction.

^{*}remi.robin@inria.fr

[†]francesco.volpe@renfusion.eu

1 Introduction

Stellarators are non-axisymmetric toroidal devices that magnetically confine fusion plasmas [2]. Thanks to specially shaped coils they do not require a current in the plasma, hence are more stable and steady-state than tokamaks. However, they exhibit comparable confinement, hence tend to be about as large. Like tokamaks, confinement can be improved (and size reduced) by adopting stronger magnetic fields.

Fields as high as 8-12 T were only tested in two series of tokamak experiments at the MIT and ENEA, culminated respectively in Alcator C-mod [3] and FTU [4]. For comparison, ITER has a field of 5.3 T on axis. Other high-field tokamaks were designed but not built [5, 6], although the new high-field SPARC tokamak has been designed, modeled and its construction is expected to start in 2021 [7].

For stellarators and heliotrons, there is broad agreement that power-plants will require at least 4-6 T [8], but fields as high as 8-12 T have only been proposed very recently [9]. Two private companies are working toward that goal [10, 11].

Generating strong fields requires high currents and of course results in high forces on the coils (unless their design is modified, as we will argue in this paper). Up to 5 T, the issue can be resolved by adequately reinforced coil-support structures and coil-spacers [12]. However, a further increase to 10 T will result in $4\times$ higher forces. This calls for including force-reduction in the coil design and optimization process, along with other criteria.

Such need was recognized earlier on for heliotrons, and spurred reduced force (so-called force-free) heliotron designs [13]. From a mathematical standpoint this is not too surprising, since helical fields in heliotrons resemble the eigenfunctions of the curl operator on a torus [14]: $\nabla \times \mathbf{B} = \lambda \mathbf{B}$. This, combined with Maxwell-Ampere law, implies that \mathbf{B} and the current density \mathbf{j} are parallel, and there are no Laplace forces on the coils.

Modular coils for advanced stellarators, on the other hand, are the result of numerical optimization. The most common optimization criterion is to reproduce the target magnetic field to within one part in 10^4 or 10^5 . Typically this is solved on a 2-D toroidal surface conformal to the plasma boundary, called Coil Winding Surface (CWS). On that surface, numerical codes compute the current potential (thus, ultimately, the current pattern) that best reproduces the target plasma boundary, in a least-squares sense [1]. This is the principle of the seminal NESCOIL code [15]. Further developments

included engineering-constrained nonlinear optimizers [16] and the Tikhonov-regularized REGCOIL [1]. The latter includes the squared coil-current density in the objective function, which leads to more “gentle”, easier-to-build coil shapes. All these codes fix the CWS; more recently, a free-CWS 3-D search method was developed [17].

In the present article, we generalize REGCOIL to include coil-force reduction. This is obtained by adding a third term to the objective function, quantifying the Laplace forces on the CWS. Several metrics are possible, for example the surface-integral of the squared Laplace force, or the peak value of the Laplace force. We recall that the Laplace forces are a self-interaction \mathbf{L} of a surface-current (of density \mathbf{j}) with itself. To that end, first we introduce the force \mathbf{L} exerted by a surface-current of density \mathbf{j}_1 on a surface-current of density \mathbf{j}_2 .

The paper is organized as follows. The Laplace force on a current-sheet is rigorously derived in Eqs. 4-7 of Section 2. The expression obtained is not overly expensive from a numerical standpoint. Based on that, possible cost functions are proposed and briefly discussed in Section 3. Finally section 4 illustrates the numerical results obtained with the two main cost-functions for the quasi-axisymmetric stellarator design formerly known as NCSX, then QUASAR, including a reduction of the peak force by up to 40%.

2 Laplace force on a surface

2.1 Limit definition of Laplace force exerted by a current-sheet on itself

In the following, S denotes the CWS and \mathbf{n} the unit vector field normal to S and pointing outward. \mathbf{j} is a vector field on S , representing the surface-current density, i.e. the current per unit length (not per unit surface, as is usually the case for this notation). The Laplace force is the magnetic component of the Lorentz force; the Laplace force per unit *surface* (not per unit volume) is given by $\mathbf{F} = \mathbf{j} \times \mathbf{B}$, although here, quite often, it will simply be called ‘force’, for brevity.

It is well-known that a surface-current causes a discontinuity in the tangential component of the magnetic field, given by the interface condition $\mathbf{n}_{12} \times (\mathbf{H}_2 - \mathbf{H}_1) = \mathbf{j}$. The resulting jump in the tangential component of \mathbf{B} results in a normal force wherever $\mathbf{j} \neq 0$. That force, proportional to $|\mathbf{j}|^2$,

tries to increase the thickness of the CWS. To ensure that that force remains reasonably small, one can easily add a cost $|\mathbf{j}|_{L^2}$ or $|\mathbf{j}|_\infty$ to the multi-objective figure-of-merit or optimize under a constraint on \mathbf{j} .

From now on, though, we will focus on the other contributions to the Laplace force. We define them in a location $\mathbf{y} \in S$ as follows:

$$\mathbf{F}(\mathbf{y}) = \lim_{\varepsilon \rightarrow 0} \frac{1}{2} \{ \mathbf{j}(\mathbf{y}) \times [\mathbf{B}(\mathbf{y} + \varepsilon \mathbf{n}(\mathbf{y})) + \mathbf{B}(\mathbf{y} - \varepsilon \mathbf{n}(\mathbf{y}))] \}.$$

Let us focus on the case where \mathbf{B} is only generated by currents on S ; there are no permanent magnets nor magnetically susceptible media. In any $\mathbf{y} \notin S$, the field is given by the Biot-Savart law in vacuo:

$$\mathbf{B}(\mathbf{y}) = \mathbf{BS}(\mathbf{j})(\mathbf{y}) = \int_S \mathbf{j}(\mathbf{x}) \times \frac{\mathbf{y} - \mathbf{x}}{|\mathbf{y} - \mathbf{x}|^3} dS(\mathbf{x}), \quad (1)$$

where, to reduce the amount of notation, we dropped the $\frac{\mu_0}{4\pi}$ factor in front of the integral. The notation $\mathbf{BS}(\mathbf{j})$ refers to the Biot-Savart operator, function of \mathbf{j} , that maps each $\mathbf{y} \notin S$ in the local field, $\mathbf{B}(\mathbf{y})$.

Remark 1. $\mathbf{BS}(\mathbf{j})$ cannot be defined on S , unless $\mathbf{j} = 0$. This is a consequence of $\frac{1}{|\mathbf{y} - \mathbf{x}|^2}$ not being integrable for $\mathbf{y} \in S$. It was expected because the interface condition introduces a discontinuity of $\mathbf{BS}(\mathbf{j})(\mathbf{y} + \varepsilon \mathbf{n}(\mathbf{y}))$ at $\varepsilon = 0$.

However, since $\mathbf{BS}(\mathbf{j})$ is well-defined in locations $\notin S$, we can define for any $\mathbf{y} \in S$ and any $\varepsilon > 0$ the bilinear map

$$\mathbf{L}_\varepsilon(\mathbf{j}_1, \mathbf{j}_2)(\mathbf{y}) = \frac{1}{2} \{ \mathbf{j}_1(\mathbf{y}) \times [\mathbf{BS}(\mathbf{j}_2)(\mathbf{y} + \varepsilon \mathbf{n}(\mathbf{y})) + \mathbf{BS}(\mathbf{j}_2)(\mathbf{y} - \varepsilon \mathbf{n}(\mathbf{y}))] \}. \quad (2)$$

This describes the Laplace force that a surface-current of density \mathbf{j}_2 exerts on another of density \mathbf{j}_1 , per unit surface. Since we are dealing with a stellarator, these currents are constant in time and there is no need to include induced fields and the associated forces.

The ‘average Laplace force’ that a current of density \mathbf{j} exerts on point $\mathbf{y} \in S$ is thus $\mathbf{L}(\mathbf{j})(\mathbf{y}) = \lim_{\varepsilon \rightarrow 0} \mathbf{L}_\varepsilon(\mathbf{j}, \mathbf{j})(\mathbf{y})$.

This definition, however, raises several questions:

1. Under which assumptions on \mathbf{j} can we ensure that $\mathbf{L}(\mathbf{j})$ is well defined (i.e., that the limit is well -defined)?
2. Can we find an explicit expression of $\mathbf{L}(\mathbf{j})$ (i.e., without a limit on ε)?

3. Which functional space does $\mathbf{L}(\mathbf{j})$ belong to (for \mathbf{j} in a given functional space)?

The first point is more theoretical, but is necessary to answer the second and third one, which have very practical consequences. Indeed, without an explicit expression for $\mathbf{L}(\mathbf{j})$, the numerical computation of the Laplace force may be a complex matter. A typical approach would involve 3 different scales. From the smallest to the largest, these are the discretisation-length of S , h , the infinitesimal displacement ε , and the characteristic distance of variation of the magnetic field, d_B .

An accurate computation of $\mathbf{B}(\mathbf{y} + \varepsilon\mathbf{n}(\mathbf{y}))$ requires S to be finely discretized, with $h \ll \varepsilon$. This is because $\int_S |\mathbf{y} + \varepsilon\mathbf{n}(\mathbf{y}) - \mathbf{x}|^{-2} dS(\mathbf{x})$ blows up when $\varepsilon \rightarrow 0$. Indeed when we replace the integral with a discrete sum and take the limit for small ε ,

$$\tilde{\mathbf{B}}(\mathbf{y}_{i,j} + \varepsilon\mathbf{n}(\mathbf{y}_{i,j})) = \sum_{k,l} \mathbf{j}(\mathbf{x}_{k,l}) \times \frac{\mathbf{y}_{i,j} + \varepsilon\mathbf{n}(\mathbf{y}_{i,j}) - \mathbf{x}_{k,l}}{|\mathbf{y}_{i,j} + \varepsilon\mathbf{n}(\mathbf{y}_{i,j}) - \mathbf{x}_{k,l}|^3} \stackrel{\varepsilon \rightarrow 0}{\approx} \frac{\mathbf{j}(\mathbf{y}_{i,j}) \times \mathbf{n}(\mathbf{y}_{i,j})}{\varepsilon^2}$$

which for small ε diverges like ε^{-2} , as shown in Figure 1 for NCSX.

The semi-sum $\frac{\mathbf{B}(\mathbf{y} + \varepsilon\mathbf{n}(\mathbf{y})) + \mathbf{B}(\mathbf{y} - \varepsilon\mathbf{n}(\mathbf{y}))}{2}$ is numerically more stable, but we still need $h \lesssim \varepsilon$ (as it will be shown later in Figure 3). Such fine mesh makes it costly to accurately compute $\mathbf{L}(\mathbf{j})(\mathbf{y})$ as $\lim_{\varepsilon \rightarrow 0} \mathbf{L}_\varepsilon(\mathbf{j}, \mathbf{j})(\mathbf{y})$.

The functional space of $\mathbf{L}(\mathbf{j})$ is also important to understand what type of penalization can be applied to minimize this force, or a related metric.

2.2 Notations

We start by introducing the following notations:

- S is a smooth 2-dimensional Riemannian submanifold of \mathbb{R}^3 , diffeomorphic to the 2-torus.
- $\mathfrak{X}(S)$ is the set of smooth vector fields on S .
- $\langle X \cdot Y \rangle$ denote the scalar product (in \mathbb{R}^3) between the vector fields X and Y . When both vector are tangent to S , we sometime denote $\langle X \cdot Y \rangle_{T_x S}$ the scalar product at $x \in S$ (which coincides with the one in \mathbb{R}^3).

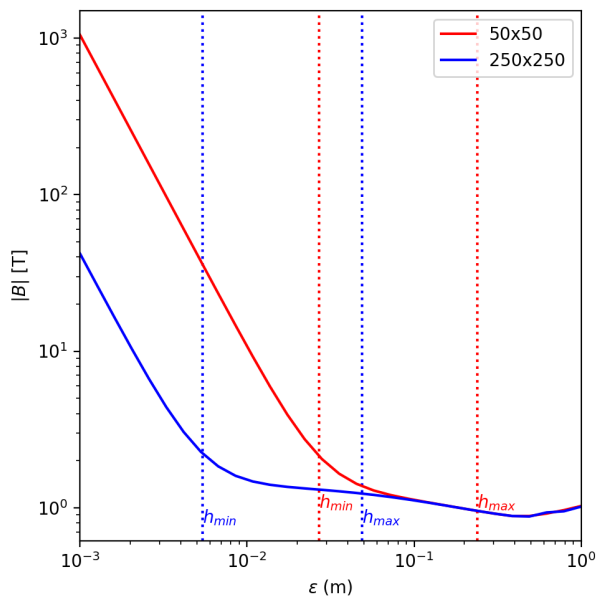


Figure 1: Average norm of \mathbf{B} as a function of the distance ε from the surface S , for two different grids, more coarse (red) or fine (blue). The divergence for small ε is a numerical artifact due to the numerical discretisation when $\varepsilon \lesssim h$.

- $L^p(S)$ and $H^1(S)$ are the Hilbert spaces defined as the completion of $\mathcal{C}^\infty(S)$ for the norms

$$|f|_{L^p(S)} = \left(\int_S f^p dS \right)^{1/p}$$

$$|f|_{H^1(S)}^2 = \int_S (f^2 + \langle \nabla f \cdot \nabla f \rangle) dS.$$

- $\mathfrak{X}^p(S)$ and $\mathfrak{X}^{1,2}(S)$ are the Hilbert spaces defined as the completion of $\mathfrak{X}(S)$ for the norms

$$|\mathbf{j}|_{\mathfrak{X}^p(S)} = \left| \sqrt{\mathbf{j}_x^2 + \mathbf{j}_y^2 + \mathbf{j}_z^2} \right|_{L^p(S)}$$

$$|\mathbf{j}|_{\mathfrak{X}^{1,2}(S)} = \sqrt{|\mathbf{j}_x|_{H^1(S)}^2 + |\mathbf{j}_y|_{H^1(S)}^2 + |\mathbf{j}_z|_{H^1(S)}^2}$$

where $\mathbf{j}_x, \mathbf{j}_y$ and \mathbf{j}_z are the components of \mathbf{j} in \mathbb{R}^3 for an arbitrary orthogonal basis.

- The spaces $L^p(S, \mathbb{R}^3)$ and $H^{1,2}(S, \mathbb{R}^3)$ are related to $\mathcal{C}^\infty(S, \mathbb{R}^3)$ in the same way as $\mathfrak{X}^p(S)$ and $\mathfrak{X}^{1,2}(S)$ are related to $\mathfrak{X}(S)$.
- π is the projector on the tangent bundle. For any $\mathbf{Y} \in \mathcal{C}^\infty(S, \mathbb{R}^3)$, we define

$$\forall \mathbf{x} \in S, (\pi(\mathbf{Y}))_{\mathbf{x}} = \mathbf{Y}_{\mathbf{x}} - \langle \mathbf{Y}_{\mathbf{x}} \cdot \mathbf{n}(\mathbf{x}) \rangle \mathbf{n}(\mathbf{x}) \in T_{\mathbf{x}}S. \quad (3)$$

Since $\pi(\mathbf{Y})$ is clearly a tangent vector field on S , it belongs to $\mathfrak{X}(S)$.

2.3 Theorem: computing the Laplace force exerted by one current-sheet on another

Theorem 1. *Let $\mathbf{j}_1, \mathbf{j}_2 \in \mathfrak{X}^{1,2}(S)$. Then $\mathbf{L}_\varepsilon(\mathbf{j}_1, \mathbf{j}_2)$ has an $\varepsilon \rightarrow 0$ limit in $L^p(S, \mathbb{R}^3)$, for any $1 \leq p < \infty$, denoted $\mathbf{L}(\mathbf{j}_1, \mathbf{j}_2)$. Furthermore, \mathbf{L} is a con-*

tinuous bilinear map $\mathfrak{X}^{1,2}(S) \times \mathfrak{X}^{1,2}(S) \rightarrow L^p(S, \mathbb{R}^3)$ given by

$$\mathbf{L}(\mathbf{j}_1, \mathbf{j}_2)(\mathbf{y}) = - \int_S \frac{1}{|\mathbf{y} - \mathbf{x}|} [\operatorname{div}_{\mathbf{x}}(\pi_{\mathbf{x}} \mathbf{j}_1(\mathbf{y})) + \pi_{\mathbf{x}} \mathbf{j}_1(\mathbf{y}) \cdot \nabla_{\mathbf{x}}] \mathbf{j}_2(\mathbf{x}) d\mathbf{x} \quad (4)$$

$$+ \int_S \langle \mathbf{j}_1(\mathbf{y}) \cdot \mathbf{n}(\mathbf{x}) \rangle \frac{\langle \mathbf{y} - \mathbf{x} \cdot \mathbf{n}(\mathbf{x}) \rangle}{|\mathbf{y} - \mathbf{x}|^3} \mathbf{j}_2(\mathbf{x}) d\mathbf{x} \quad (5)$$

$$+ \int_S \frac{1}{|\mathbf{y} - \mathbf{x}|} [\langle \mathbf{j}_1(\mathbf{y}) \cdot \mathbf{j}_2(\mathbf{x}) \rangle \operatorname{div}_{\mathbf{x}}(\pi_{\mathbf{x}}) + \nabla_{\mathbf{x}} \langle \mathbf{j}_1(\mathbf{y}) \cdot \mathbf{j}_2(\mathbf{x}) \rangle] d\mathbf{x} \quad (6)$$

$$- \int_S \langle \mathbf{j}_1(\mathbf{y}) \cdot \mathbf{j}_2(\mathbf{x}) \rangle \frac{\langle \mathbf{y} - \mathbf{x} \cdot \mathbf{n}(\mathbf{x}) \rangle}{|\mathbf{y} - \mathbf{x}|^3} \mathbf{n}(\mathbf{x}) d\mathbf{x} \quad (7)$$

Remark 2. • The notation $V \cdot \nabla_{\mathbf{x}} F$ (where $V \in \mathfrak{X}(S)$ is a 2D vector and $F \in C^\infty(S, \mathbb{R}^3)$ a 3D one) stands for $\sum_{\alpha=1}^2 \sum_{i=1}^3 V^\alpha \partial_\alpha F^i \mathbf{e}_i$. Here α is the index for the surface coordinates (θ and φ , for example), whereas $(\mathbf{e}_1, \mathbf{e}_2, \mathbf{e}_3)$ is a basis of \mathbb{R}^3 .

- $\operatorname{div}_{\mathbf{x}}(\pi_{\mathbf{x}})$ stands for the 3D vector $\sum_{i=1}^3 \operatorname{div}_{\mathbf{x}}(\pi_{\mathbf{x}} \mathbf{e}_i) \mathbf{e}_i$

The proof of the theorem is somewhat long and will be organized as follows: in Sec. 2.3.1 we will rewrite Eq. 2 in terms of surface integrals 13, 14, 17 and 18. Integrals 13 and 17, with integrands tangential to S (“tangential terms”) will be dealt with in Sec. 2.3.2 and 2.3.3. Integrals 14 and 18, with integrands normal to S (“normal terms”) will be treated in Sec. 2.3.4 and 2.3.5.

2.3.1 Proof: beginning and general ideas

Consider two linear densities of surface-currents $\mathbf{j}_1, \mathbf{j}_2 \in \mathfrak{X}^{1,2}(S)$ and fix $\epsilon > 0$.

Thanks to the well-known formula $\mathbf{A} \times (\mathbf{B} \times \mathbf{C}) = (\mathbf{A} \cdot \mathbf{C})\mathbf{B} - (\mathbf{A} \cdot \mathbf{B})\mathbf{C}$, we obtain from Eqs.1 and 2 that

$$\mathbf{L}_\epsilon(\mathbf{j}_1, \mathbf{j}_2)(\mathbf{y}) = \int_S \langle \mathbf{j}_1(\mathbf{y}) \cdot \left(\frac{\mathbf{y} - \mathbf{x} + \epsilon \mathbf{n}(\mathbf{y})}{2|\mathbf{y} - \mathbf{x} + \epsilon \mathbf{n}(\mathbf{y})|^3} + \frac{\mathbf{y} - \mathbf{x} - \epsilon \mathbf{n}(\mathbf{y})}{2|\mathbf{y} - \mathbf{x} - \epsilon \mathbf{n}(\mathbf{y})|^3} \right) \rangle \mathbf{j}_2(\mathbf{x}) d\mathbf{x} \quad (8)$$

$$- \int_S \langle \mathbf{j}_1(\mathbf{y}) \cdot \mathbf{j}_2(\mathbf{x}) \rangle \left(\frac{\mathbf{y} - \mathbf{x} + \epsilon \mathbf{n}(\mathbf{y})}{2|\mathbf{y} - \mathbf{x} + \epsilon \mathbf{n}(\mathbf{y})|^3} + \frac{\mathbf{y} - \mathbf{x} - \epsilon \mathbf{n}(\mathbf{y})}{2|\mathbf{y} - \mathbf{x} - \epsilon \mathbf{n}(\mathbf{y})|^3} \right) d\mathbf{x}. \quad (9)$$

The difficulty is that $\frac{1}{|x|^2}$ is not integrable in 2 dimensions (Remark 1). Hence, it does not make sense to take the limit for $\varepsilon \rightarrow 0$ directly inside the integral. Nevertheless, we can use the following equality:

$$\int_S \langle \mathbf{j}_1(\mathbf{y}) \cdot \frac{\mathbf{y} - \mathbf{x} + \varepsilon \mathbf{n}(\mathbf{y})}{|\mathbf{y} - \mathbf{x} + \varepsilon \mathbf{n}(\mathbf{y})|^3} \rangle \mathbf{j}_2(\mathbf{x}) d\mathbf{x} = \int_S \langle \mathbf{j}_1(\mathbf{y}) \cdot \nabla_{\mathbf{x}} \frac{1}{|\mathbf{y} - \mathbf{x} + \varepsilon \mathbf{n}(\mathbf{y})|} \rangle \mathbf{j}_2(\mathbf{x}) d\mathbf{x} \quad (10)$$

where $\nabla_{\mathbf{x}}$ is the gradient in \mathbb{R}^3 with respect to the variable \mathbf{x} . We would like to integrate by part to take advantage of the integrability of $\frac{1}{|x|}$. For this we decompose $\nabla_{\mathbf{x}}$ into the tangential part of the gradient, ∇_S , and normal component, ∇_{\perp} . As a consequence, for Eq. 8 we have the following equalities:

$$\int_S \langle \mathbf{j}_1(\mathbf{y}) \cdot \frac{\mathbf{y} - \mathbf{x} \pm \varepsilon \mathbf{n}(\mathbf{y})}{|\mathbf{y} - \mathbf{x} \pm \varepsilon \mathbf{n}(\mathbf{y})|^3} \rangle \mathbf{j}_2(\mathbf{x}) d\mathbf{x} \quad (11)$$

$$= \int_S \langle \mathbf{j}_1(\mathbf{y}) \cdot \nabla_{\mathbf{x}} \frac{1}{|\mathbf{y} - \mathbf{x} \pm \varepsilon \mathbf{n}(\mathbf{y})|} \rangle \mathbf{j}_2(\mathbf{x}) d\mathbf{x} \quad (12)$$

$$= \int_S \langle \mathbf{j}_1(\mathbf{y}) \cdot \nabla_S \frac{1}{|\mathbf{y} - \mathbf{x} \pm \varepsilon \mathbf{n}(\mathbf{y})|} \rangle \mathbf{j}_2(\mathbf{x}) d\mathbf{x} \quad (13)$$

$$+ \int_S \langle \mathbf{j}_1(\mathbf{y}) \cdot \frac{\langle \mathbf{y} - \mathbf{x}, \mathbf{n}(\mathbf{x}) \rangle \pm \varepsilon \langle \mathbf{n}(\mathbf{y}), \mathbf{n}(\mathbf{x}) \rangle}{|\mathbf{y} - \mathbf{x} \pm \varepsilon \mathbf{n}(\mathbf{y})|^3} \mathbf{n}(\mathbf{x}) \rangle \mathbf{j}_2(\mathbf{x}) d\mathbf{x} \quad (14)$$

and for expression 9

$$\int_S \langle \mathbf{j}_1(\mathbf{y}) \cdot \mathbf{j}_2(\mathbf{x}) \rangle \frac{\mathbf{y} - \mathbf{x} \pm \varepsilon \mathbf{n}(\mathbf{y})}{|\mathbf{y} - \mathbf{x} \pm \varepsilon \mathbf{n}(\mathbf{y})|^3} d\mathbf{x} \quad (15)$$

$$= \int_S \langle \mathbf{j}_1(\mathbf{y}) \cdot \mathbf{j}_2(\mathbf{x}) \rangle \nabla_{\mathbf{x}} \frac{1}{|\mathbf{y} - \mathbf{x} \pm \varepsilon \mathbf{n}(\mathbf{y})|} d\mathbf{x} \quad (16)$$

$$= \int_S \langle \mathbf{j}_1(\mathbf{y}) \cdot \mathbf{j}_2(\mathbf{x}) \rangle \nabla_S \frac{1}{|\mathbf{y} - \mathbf{x} \pm \varepsilon \mathbf{n}(\mathbf{y})|} d\mathbf{x} \quad (17)$$

$$+ \int_S \langle \mathbf{j}_1(\mathbf{y}) \cdot \mathbf{j}_2(\mathbf{x}) \rangle \frac{\langle \mathbf{y} - \mathbf{x}, \mathbf{n}(\mathbf{x}) \rangle \pm \varepsilon \langle \mathbf{n}(\mathbf{y}), \mathbf{n}(\mathbf{x}) \rangle}{|\mathbf{y} - \mathbf{x} \pm \varepsilon \mathbf{n}(\mathbf{y})|^3} \mathbf{n}(\mathbf{x}) d\mathbf{x} \quad (18)$$

2.3.2 Proof: First tangential term

Integration by parts on a compact manifold \mathcal{M} without boundary is given by the following formula. Let $f \in \mathcal{C}^\infty(\mathcal{M})$ and \mathbf{X} a smooth vector field on \mathcal{M} , then

$$\int_{\mathcal{M}} \operatorname{div}(f\mathbf{X}) = 0 = \mathbf{X}f + \int_{\mathcal{M}} f \operatorname{div} \mathbf{X} \quad (19)$$

We also recall that $\mathbf{X}f = \langle \mathbf{X} \cdot \nabla f \rangle$ in Euclidean coordinates.

Let us start with the first tangential term (Eq. 13):

$$\begin{aligned} & \int_S \langle \mathbf{j}_1(\mathbf{y}) \cdot \nabla_S \frac{1}{|\mathbf{y} - \mathbf{x} \pm \varepsilon \mathbf{n}(\mathbf{y})|} \rangle_{\mathbb{R}^3} \mathbf{j}_2(\mathbf{x}) d\mathbf{x} \\ &= \int_S \langle \pi_{\mathbf{x}} \mathbf{j}_1(\mathbf{y}) \cdot \nabla_S \frac{1}{|\mathbf{y} - \mathbf{x} \pm \varepsilon \mathbf{n}(\mathbf{y})|} \rangle_{T_x S} \mathbf{j}_2(\mathbf{x}) d\mathbf{x} \end{aligned}$$

as $\mathbf{j}_1(\mathbf{y}) - \pi_{\mathbf{x}} \mathbf{j}_1(\mathbf{y}) \propto \mathbf{n}(\mathbf{x})$.

Then, let $j_2^i(\mathbf{x})$ be the i -th component in \mathbb{R}^3 of \mathbf{j}_2 . Using integration by parts (Eq. 19), the i -th component of the last integral writes

$$\int_S \langle j_2^i(\mathbf{x}) \pi_{\mathbf{x}} \mathbf{j}_1(\mathbf{y}) \cdot \nabla_S \frac{1}{|\mathbf{y} - \mathbf{x} \pm \varepsilon \mathbf{n}(\mathbf{y})|} \rangle_{T_x S} d\mathbf{x} \quad (20)$$

$$= - \int_S \frac{1}{|\mathbf{y} - \mathbf{x} \pm \varepsilon \mathbf{n}(\mathbf{y})|} \operatorname{div}_{\mathbf{x}}(j_2^i(\mathbf{x}) \pi_{\mathbf{x}} \mathbf{j}_1(\mathbf{y})) d\mathbf{x} \quad (21)$$

$$= - \int_S \frac{1}{|\mathbf{y} - \mathbf{x} \pm \varepsilon \mathbf{n}(\mathbf{y})|} [j_2^i(\mathbf{x}) \operatorname{div}_{\mathbf{x}}(\pi_{\mathbf{x}} \mathbf{j}_1(\mathbf{y})) + \langle \pi_{\mathbf{x}} \mathbf{j}_1(\mathbf{y}) \cdot \nabla j_2^i(\mathbf{x}) \rangle] d\mathbf{x} \quad (22)$$

Thus the term in equation 10 is equal to:

$$- \sum_{i=1}^3 \left(\int_S \frac{1}{|\mathbf{y} - \mathbf{x} \pm \varepsilon \mathbf{n}(\mathbf{y})|} [j_2^i(\mathbf{x}) \operatorname{div}_{\mathbf{x}}(\pi_{\mathbf{x}} \mathbf{j}_1(\mathbf{y})) + \langle \pi_{\mathbf{x}} \mathbf{j}_1(\mathbf{y}) \cdot \nabla j_2^i(\mathbf{x}) \rangle] d\mathbf{x} \right) \mathbf{e}_i$$

that, with the conventions introduced in Remark 2, can be rewritten as:

$$- \int_S \frac{1}{|\mathbf{y} - \mathbf{x} \pm \varepsilon \mathbf{n}(\mathbf{y})|} [\operatorname{div}_{\mathbf{x}}(\pi_{\mathbf{x}} \mathbf{j}_1(\mathbf{y})) + \pi_{\mathbf{x}} \mathbf{j}_1(\mathbf{y}) \cdot \nabla_{\mathbf{x}}] \mathbf{j}_2(\mathbf{x}) d\mathbf{x}$$

Now, we will prove that it is possible to take the limit $\varepsilon \rightarrow 0$ inside this integral. The first step is to use the following estimate.

Lemma 1. $|\operatorname{div}_{\mathbf{x}} \pi_{\mathbf{x}} \mathbf{j}_1(\mathbf{y})| \leq C(S) |\mathbf{j}_1(\mathbf{y})|$ with $C(S)$ a constant that only depends on the metric of S .

Proof. Indeed, the application

$$\begin{aligned} \operatorname{div}_{\mathbf{x}} \pi_{\mathbf{x}}: \mathbb{R}^3 &\rightarrow \mathcal{C}^\infty(S) \\ \mathbf{v} &\mapsto (\mathbf{x} \mapsto \operatorname{div}_{\mathbf{x}}(\pi_{\mathbf{x}} \mathbf{v})). \end{aligned}$$

is a continuous linear application. □

We also need a Young-type inequality for 2-dimensional compact manifolds.

Lemma 2. *For all $1 \leq q < \infty$, there exists $C > 0$ such that for all f in $L^2(S)$, $|\int_S \frac{1}{|\mathbf{y}-\mathbf{x}|} f(\mathbf{x}) d\mathbf{x}|_{L^q_y} \leq C_q |f|_{L^2}$.*

Proof. Let d_g denote the Riemannian distance on S . By a Hardy-Littlewood-Sobolev inequality $\int_S \frac{1}{d_g(\mathbf{y},\mathbf{x})} f(x) d\mathbf{x}$ is in $L^q(S)$ for all $1 \leq q < \infty$. This result can be found, for example, in [18] or can be proved directly with the arguments of the proof of the classical Young inequality. As the Euclidean distance and the Riemannian distance are equivalent, the lemma is proved. \square

Thus, for all $1 \leq q < \infty$, $\int_S \frac{1}{|\mathbf{y}-\mathbf{x}|} \partial_i \mathbf{j}_2(\mathbf{x}) d\mathbf{x} \in L^q(S, \mathbb{R}^3)$. Besides, by Sobolev embedding [19], there is a continuous injection $\mathfrak{X}^{1,2}(S) \hookrightarrow \mathfrak{X}^p(S)$ for all $1 \leq p < \infty$. As a consequence $j_1^i(\mathbf{y}) \int_S \frac{1}{|\mathbf{y}-\mathbf{x}|} \partial_i \mathbf{j}_2(\mathbf{x}) d\mathbf{x} \in \mathfrak{X}^p(S)$ for $1 \leq p < \infty$.

With these estimates we can conclude, using dominated convergence, that:

$$\int_S \langle \mathbf{j}_1(\mathbf{y}) \cdot \nabla_S \frac{1}{|\mathbf{y}-\mathbf{x} \pm \varepsilon \mathbf{n}(\mathbf{y})|} \rangle \mathbf{j}_2(\mathbf{x}) d\mathbf{x} \quad (23)$$

$$\xrightarrow{\mathfrak{X}^p(S)} - \int_S \frac{1}{|\mathbf{y}-\mathbf{x}|} \operatorname{div}_{\mathbf{x}}(\pi_{\mathbf{x}} \mathbf{j}_1(\mathbf{y})) \mathbf{j}_2(\mathbf{x}) d\mathbf{x} \quad (24)$$

$$- \int_S \frac{1}{|\mathbf{y}-\mathbf{x}|} (\pi_{\mathbf{x}} \mathbf{j}_1(\mathbf{y}) \cdot \nabla_{\mathbf{x}}) \mathbf{j}_2(\mathbf{x}) d\mathbf{x} \quad (25)$$

Note that the two integrals (respectively with the sign + or - at denominator) converge to the same limit. Their sum yields the integral on the right-hand-side of Eq. 4.

2.3.3 Proof: Second tangential term

Now, let us tackle the term in Eq. 17. We start by computing the i -th component of that integral, i.e. its projection on \mathbf{e}_i , then follow a derivation

similar to Eqs. 20-22:

$$\begin{aligned}
& \int_S \langle \mathbf{j}_1(\mathbf{y}) \cdot \mathbf{j}_2(\mathbf{x}) \rangle \langle \mathbf{e}_i \cdot \nabla_S \frac{1}{|\mathbf{y} - \mathbf{x} \pm \varepsilon \mathbf{n}(\mathbf{y})|} \rangle d\mathbf{x} \\
&= \int_S \langle \mathbf{j}_1(\mathbf{y}) \cdot \mathbf{j}_2(\mathbf{x}) \rangle \langle \pi_{\mathbf{x}} \mathbf{e}_i \cdot \nabla_S \frac{1}{|\mathbf{y} - \mathbf{x} \pm \varepsilon \mathbf{n}(\mathbf{y})|} \rangle d\mathbf{x} \\
&= - \int_S \frac{1}{|\mathbf{y} - \mathbf{x} \pm \varepsilon \mathbf{n}(\mathbf{y})|} \operatorname{div}_{\mathbf{x}} (\langle \mathbf{j}_1(\mathbf{y}) \cdot \mathbf{j}_2(\mathbf{x}) \rangle \pi_{\mathbf{x}} \mathbf{e}_i) d\mathbf{x} \\
&= - \int_S \frac{1}{|\mathbf{y} - \mathbf{x} \pm \varepsilon \mathbf{n}(\mathbf{y})|} [\langle \mathbf{j}_1(\mathbf{y}) \cdot \mathbf{j}_2(\mathbf{x}) \rangle \operatorname{div}_{\mathbf{x}} (\pi_{\mathbf{x}} \mathbf{e}_i) + \langle \pi_{\mathbf{x}} \mathbf{e}_i \cdot \nabla_{\mathbf{x}} \langle \mathbf{j}_1(\mathbf{y}) \cdot \mathbf{j}_2(\mathbf{x}) \rangle \rangle] d\mathbf{x}.
\end{aligned}$$

Using the notation of Remark 2, we find the vector form of the integral:

$$- \int_S \frac{1}{|\mathbf{y} - \mathbf{x} \pm \varepsilon \mathbf{n}(\mathbf{y})|} (\langle \mathbf{j}_1(\mathbf{y}) \cdot \mathbf{j}_2(\mathbf{x}) \rangle \operatorname{div}_{\mathbf{x}} (\pi_{\mathbf{x}}) + \nabla_{\mathbf{x}} \langle \mathbf{j}_1(\mathbf{y}) \cdot \mathbf{j}_2(\mathbf{x}) \rangle) d\mathbf{x}.$$

Due to the same arguments invoked in Eqs. 23-25, both integrals, with the sign + and - at denominator, converge in $\mathfrak{X}^p(S)$ to the same limit,

$$- \int_S \frac{1}{|\mathbf{y} - \mathbf{x}|} [\langle \mathbf{j}_1(\mathbf{y}) \cdot \mathbf{j}_2(\mathbf{x}) \rangle \operatorname{div}_{\mathbf{x}} (\pi_{\mathbf{x}}) + \nabla_{\mathbf{x}} \langle \mathbf{j}_1(\mathbf{y}) \cdot \mathbf{j}_2(\mathbf{x}) \rangle] d\mathbf{x}.$$

Their sum yields integral 6.

2.3.4 Proof: First normal term

Let us now focus on the normal component of 8, namely Eq. 14. This is in effect the sum of two integrals, which we will discuss separately:

$$\int_S \langle \mathbf{j}_1(\mathbf{y}) \cdot \mathbf{n}(\mathbf{x}) \rangle \frac{\langle \mathbf{y} - \mathbf{x}, \mathbf{n}(\mathbf{x}) \rangle}{|\mathbf{y} - \mathbf{x} \pm \varepsilon \mathbf{n}(\mathbf{y})|^3} \mathbf{j}_2(\mathbf{x}) d\mathbf{x} \quad (26)$$

$$\int_S \langle \mathbf{j}_1(\mathbf{y}) \cdot \mathbf{n}(\mathbf{x}) \rangle \frac{\pm \varepsilon \langle \mathbf{n}(\mathbf{y}), \mathbf{n}(\mathbf{x}) \rangle}{|\mathbf{y} - \mathbf{x} \pm \varepsilon \mathbf{n}(\mathbf{y})|^3} \mathbf{j}_2(\mathbf{x}) d\mathbf{x} \quad (27)$$

First notice that we have the following estimate:

Lemma 3. $\exists C > 0, \forall \mathbf{x} \neq \mathbf{y} \in S, \frac{|\langle \mathbf{y} - \mathbf{x}, \mathbf{n}(\mathbf{x}) \rangle|}{|\mathbf{y} - \mathbf{x}|^2} \leq C.$

Proof. Let us suppose there exist two sequences $(\mathbf{x}_n), (\mathbf{y}_n)$ in S such that $\mathbf{x}_n \neq \mathbf{y}_n$ and $\frac{|\langle \mathbf{y}_n - \mathbf{x}_n, \mathbf{n}(\mathbf{x}_n) \rangle|}{|\mathbf{y}_n - \mathbf{x}_n|^2} \rightarrow \infty.$ Up to an extraction, we can suppose that

$\mathbf{x}_n \rightarrow \mathbf{x}_0 \in S$. If \mathbf{y}_n does not converges to \mathbf{x}_0 , we can extract a subsequence such that $\frac{|\langle \mathbf{y}_n - \mathbf{x}_n, \mathbf{n}(\mathbf{x}_n) \rangle|}{|\mathbf{y}_n - \mathbf{x}_n|^2}$ does not diverge. This is a contradiction, hence both \mathbf{x}_n and \mathbf{y}_n converge to $\mathbf{x}_0 \in S$.

Let $\Gamma(\mathbf{x}, \mathbf{y}) = \langle \mathbf{y} - \mathbf{x}, \mathbf{n}(\mathbf{x}) \rangle$. As S is smooth, so is Γ . Its partial differentials are

$$\begin{aligned} \forall \mathbf{h} \in T_{\mathbf{x}}S, \quad d_{\mathbf{x}}\Gamma_{\mathbf{x},\mathbf{y}}(\mathbf{h}) &= -\langle -\mathbf{h} \cdot \mathbf{n}(\mathbf{x}) \rangle + \langle \mathbf{y} - \mathbf{x} \cdot d\mathbf{n}_{\mathbf{x}}(\mathbf{h}) \rangle \\ \forall \mathbf{h} \in T_{\mathbf{y}}S, \quad d_{\mathbf{y}}\Gamma_{\mathbf{x},\mathbf{y}}(\mathbf{h}) &= \langle \mathbf{h} \cdot \mathbf{n}(\mathbf{x}) \rangle \end{aligned}$$

Thus, at the point $(\mathbf{x}_0, \mathbf{x}_0)$, both first derivatives vanish. As a consequence, for n big enough there exists $C > 0$ such that $\Gamma(\mathbf{x}_n, \mathbf{y}_n) \leq C|\mathbf{x}_n - \mathbf{y}_n|^2$, contradiction. \square

Now, we need to find a minoration of $|\mathbf{y} - \mathbf{x} \pm \varepsilon \mathbf{n}(\mathbf{y})|$.

Lemma 4. *For ε small enough, for all $\mu > 0$,*

$$|\mathbf{x} - \mathbf{y} \pm \varepsilon \mathbf{n}(\mathbf{y})|^\mu \geq \max\left(\left(\frac{1}{\sqrt{2}}|\mathbf{x} - \mathbf{y}|\right)^\mu, \varepsilon^\mu\right).$$

Proof.

$$\begin{aligned} |\mathbf{y} - \mathbf{x} \pm \varepsilon \mathbf{n}(\mathbf{y})|^2 &= |\mathbf{y} - \mathbf{x}|^2 \pm \varepsilon \langle \mathbf{y} - \mathbf{x}, \mathbf{n}(\mathbf{y}) \rangle + \varepsilon^2 \\ &\geq |\mathbf{y} - \mathbf{x}|^2 - C\varepsilon |\mathbf{y} - \mathbf{x}|^2 + \varepsilon^2 \quad \text{by lemma 3.} \end{aligned}$$

Thus for $\varepsilon \leq 1/(2C)$, we have, $\forall \mu > 0$,

$$|\mathbf{x} - \mathbf{y} \pm \varepsilon \mathbf{n}(\mathbf{y})|^\mu \geq \max\left(\left(\frac{1}{\sqrt{2}}|\mathbf{x} - \mathbf{y}|\right)^\mu, \varepsilon^\mu\right).$$

\square

Using Lemmas 3 and 4, for some constant C , $\left|\frac{\langle \mathbf{y} - \mathbf{x}, \mathbf{n}(\mathbf{x}) \rangle}{|\mathbf{y} - \mathbf{x} \pm \varepsilon \mathbf{n}(\mathbf{y})|^3}\right|$ is dominated by $C\frac{1}{|\mathbf{y} - \mathbf{x}|}$, which is integrable. By dominated convergence

$$\int_S \langle \mathbf{j}_1(\mathbf{y}) \cdot \mathbf{n}(\mathbf{x}) \rangle \frac{\langle \mathbf{y} - \mathbf{x}, \mathbf{n}(\mathbf{x}) \rangle}{|\mathbf{y} - \mathbf{x} \pm \varepsilon \mathbf{n}(\mathbf{y})|^3} \mathbf{j}_2(\mathbf{x}) d\mathbf{x} \xrightarrow{\varepsilon \rightarrow 0} \int_S \langle \mathbf{j}_1(\mathbf{y}) \cdot \mathbf{n}(\mathbf{x}) \rangle \frac{\langle \mathbf{y} - \mathbf{x}, \mathbf{n}(\mathbf{x}) \rangle}{|\mathbf{y} - \mathbf{x}|^3} \mathbf{j}_2(\mathbf{x}) d\mathbf{x}, \quad (28)$$

i.e. we obtained integral 5.

Now we have to deal with $\frac{\varepsilon \langle \mathbf{n}(\mathbf{y}), \mathbf{n}(\mathbf{x}) \rangle}{|\mathbf{y} - \mathbf{x} \pm \varepsilon \mathbf{n}(\mathbf{y})|^3}$, but we will show their net contribution to converge to zero.

To begin with, we could use the smallness of the term $\langle \mathbf{j}_1(\mathbf{y}) \cdot \mathbf{n}(\mathbf{x}) \rangle$ to ensure integrability. Instead, we will prove the following lemma which will also be useful later. Let $\Delta = \{(\mathbf{z}, \mathbf{z}) \mid \mathbf{z} \in S\} \subset S^2$.

Lemma 5. Let $f_\varepsilon : S^2 \setminus \Delta \ni (\mathbf{x}, \mathbf{y}) \mapsto \frac{1}{|\mathbf{y}-\mathbf{x}+\varepsilon\mathbf{n}(\mathbf{y})|^3} - \frac{1}{|\mathbf{y}-\mathbf{x}-\varepsilon\mathbf{n}(\mathbf{y})|^3} d\mathbf{x}$. Then $\exists \eta > 0, \exists M > 0, \forall \alpha \in (-0.5, 3.5), \forall \varepsilon < \eta, \forall (\mathbf{x}, \mathbf{y}), |\varepsilon^\alpha f_\varepsilon(\mathbf{x}, \mathbf{y})| \leq M \frac{1}{|\mathbf{x}-\mathbf{y}|^{5/2-\alpha}}$.

Proof.

$$\begin{aligned} f_\varepsilon(\mathbf{x}, \mathbf{y}) &= \frac{|\mathbf{y}-\mathbf{x}-\varepsilon\mathbf{n}(\mathbf{y})|^3 - |\mathbf{y}-\mathbf{x}+\varepsilon\mathbf{n}(\mathbf{y})|^3}{|\mathbf{y}-\mathbf{x}+\varepsilon\mathbf{n}(\mathbf{y})|^3 |\mathbf{y}-\mathbf{x}-\varepsilon\mathbf{n}(\mathbf{y})|^3} \\ &= (|\mathbf{y}-\mathbf{x}-\varepsilon\mathbf{n}(\mathbf{y})| - |\mathbf{y}-\mathbf{x}+\varepsilon\mathbf{n}(\mathbf{y})|) \times \\ &\quad \frac{(|\mathbf{y}-\mathbf{x}+\varepsilon\mathbf{n}(\mathbf{y})|^2 + |\mathbf{y}-\mathbf{x}+\varepsilon\mathbf{n}(\mathbf{y})| |\mathbf{y}-\mathbf{x}-\varepsilon\mathbf{n}(\mathbf{y})| + |\mathbf{y}-\mathbf{x}-\varepsilon\mathbf{n}(\mathbf{y})|^2)}{|\mathbf{y}-\mathbf{x}+\varepsilon\mathbf{n}(\mathbf{y})|^3 |\mathbf{y}-\mathbf{x}-\varepsilon\mathbf{n}(\mathbf{y})|^3} \end{aligned}$$

Using the fact that square root is 1/2-Hölder ($a \geq b \geq 0, \sqrt{a} - \sqrt{b} \leq \sqrt{a-b}$) and Lemma 3, there exists $C > 0$ such that

$$||\mathbf{y}-\mathbf{x}+\varepsilon\mathbf{n}(\mathbf{y})| - |\mathbf{y}-\mathbf{x}-\varepsilon\mathbf{n}(\mathbf{y})|| \leq 2\sqrt{\varepsilon|\langle \mathbf{x}-\mathbf{y}, \mathbf{n}(\mathbf{y}) \rangle|} \leq C\sqrt{\varepsilon}|\mathbf{x}-\mathbf{y}|$$

Now we use the minoration of the denominator from Lemma 4. Up to a global multiplicative constant M , we get, for any $0 \leq \nu \leq 4$,

$$\begin{aligned} |f_\varepsilon(\mathbf{x}, \mathbf{y})| &\leq 4C \frac{\sqrt{\varepsilon}|\mathbf{x}-\mathbf{y}|}{|\mathbf{x}-\mathbf{y}|^{4-\nu}\varepsilon^\nu} \\ &\leq M \frac{1}{\varepsilon^\alpha |\mathbf{x}-\mathbf{y}|^{5/2-\alpha}} \end{aligned}$$

for any $-0.5 \leq \alpha \leq 3.5$ □

Thanks to Lemma 5 with any $\alpha \in (1/2, 1)$, there exists $C > 0$ such that

$$\left| \int_S \left(\frac{\varepsilon \langle \mathbf{n}(\mathbf{y}), \mathbf{n}(\mathbf{x}) \rangle}{|\mathbf{y}-\mathbf{x}+\varepsilon\mathbf{n}(\mathbf{y})|^3} - \frac{\varepsilon \langle \mathbf{n}(\mathbf{y}), \mathbf{n}(\mathbf{x}) \rangle}{|\mathbf{y}-\mathbf{x}-\varepsilon\mathbf{n}(\mathbf{y})|^3} \right) \mathbf{j}_2(\mathbf{x}) d\mathbf{x} \right|_{\mathbb{R}^3} \leq C \int_S \frac{\varepsilon}{\varepsilon^\alpha |\mathbf{x}-\mathbf{y}|^{5/2-\alpha}} |\mathbf{j}_2|.$$

Using an Hardy-Littlewood-Sobolev inequality (e.g. [18]) for $1 \leq p < \infty$, there exists $C_\alpha > 0$ such that

$$\left| \int_S \left(\frac{\varepsilon \langle \mathbf{n}(\mathbf{y}), \mathbf{n}(\mathbf{x}) \rangle}{|\mathbf{y}-\mathbf{x}+\varepsilon\mathbf{n}(\mathbf{y})|^3} - \frac{\varepsilon \langle \mathbf{n}(\mathbf{y}), \mathbf{n}(\mathbf{x}) \rangle}{|\mathbf{y}-\mathbf{x}-\varepsilon\mathbf{n}(\mathbf{y})|^3} \right) \mathbf{j}_2(\mathbf{x}) d\mathbf{x} \right|_{\mathbb{R}^p(S)} \leq C_\alpha \varepsilon^{1-\alpha} |\mathbf{j}_2|_{\mathbb{R}^{1,2}(S)}.$$

Thus

$$\int_S \langle \mathbf{j}_1(\mathbf{y}) \cdot \mathbf{n}(\mathbf{x}) \rangle \left(\frac{\varepsilon \langle \mathbf{n}(\mathbf{y}), \mathbf{n}(\mathbf{x}) \rangle}{|\mathbf{y}-\mathbf{x}+\varepsilon\mathbf{n}(\mathbf{y})|^3} - \frac{\varepsilon \langle \mathbf{n}(\mathbf{y}), \mathbf{n}(\mathbf{x}) \rangle}{|\mathbf{y}-\mathbf{x}-\varepsilon\mathbf{n}(\mathbf{y})|^3} \right) \mathbf{j}_2(\mathbf{x}) d\mathbf{x} \xrightarrow{\mathbb{R}^p(S)} 0 \quad (29)$$

In summary, Eq. 14 is the sum of two integrals converging respectively as in Eq. 28 and 29. Ultimately the “first normal term” converges to Eq. 5.

2.3.5 Proof: Second normal term

The same reasoning just applied to integral 14 also applies to integral 18,

$$\int_S \langle \mathbf{j}_1(\mathbf{y}) \cdot \mathbf{j}_2(\mathbf{x}) \rangle \frac{\langle \mathbf{y} - \mathbf{x}, \mathbf{n}(\mathbf{x}) \rangle \pm \varepsilon \langle \mathbf{n}(\mathbf{y}), \mathbf{n}(\mathbf{x}) \rangle}{|\mathbf{y} - \mathbf{x} \pm \varepsilon \mathbf{n}(\mathbf{y})|^3} d\mathbf{x},$$

which converges to

$$\int_S \langle \mathbf{j}_1(\mathbf{y}) \cdot \mathbf{j}_2(\mathbf{x}) \rangle \frac{\langle \mathbf{y} - \mathbf{x}, \mathbf{n}(\mathbf{x}) \rangle}{|\mathbf{y} - \mathbf{x}|^3} d\mathbf{x},$$

i.e. to Eq. 7.

This concludes the proof of Theorem 1: one by one, in Secs. 2.3.2-2.3.5, we have obtained all terms in Eqs. 4-7.

Note that we do not expect $\int_S \langle \mathbf{j}_1(\mathbf{y}) \cdot \mathbf{j}_2(\mathbf{x}) \rangle \frac{\varepsilon \langle \mathbf{n}(\mathbf{y}), \mathbf{n}(\mathbf{x}) \rangle}{|\mathbf{y} - \mathbf{x} + \varepsilon \mathbf{n}(\mathbf{y})|^3} d\mathbf{x}$ to go to 0 as that term is responsible for the magnetic field discontinuity. But we are still able to use Lemma 5 to control the term $\frac{\varepsilon}{|\mathbf{y} - \mathbf{x} + \varepsilon \mathbf{n}(\mathbf{y})|^3} - \frac{\varepsilon}{|\mathbf{y} - \mathbf{x} - \varepsilon \mathbf{n}(\mathbf{y})|^3}$.

Remark 3. *We do not expect $\mathbf{L}(\mathbf{j}_1, \mathbf{j}_2)$ to be in $L^\infty(S, \mathbb{R}^3)$. Indeed, $H^1(S)$ is not embedded in $L^\infty(S)$ for manifolds of dimension 2. For example, there is no constant $C > 0$ such that $|\int_S \frac{1}{|\mathbf{y} - \mathbf{x}|} \operatorname{div}_{\mathbf{x}}(\pi_{\mathbf{x}} \mathbf{j}_1(\mathbf{y})) \mathbf{j}_2(\mathbf{x}) d\mathbf{x}|_{L^\infty(S, \mathbb{R}^3)} \leq C |\mathbf{j}_1|_{\mathcal{X}^{1,2}(S)}$.*

2.4 Justification from a 3D current modelisation

Recapitulating, the Laplace force has been initially defined as the $\varepsilon \rightarrow 0$ limit of the semi-sum of the magnetic field evaluated at a distance ε away from the CWS, S , respectively inward and outward (Eq. 2). This was shown to either be numerically costly or subject to numerical errors (Figure 1).

An expression (Eqs. 4-7) has then been derived in Theorem 1 for the Laplace force exerted by one current-sheet on another, per unit length. The special case $\mathbf{j}_1 = \mathbf{j}_2$ describes the self-interaction of a current-sheet.

Both treatments relied on an intrinsically 2D model for the currents on the CWS. A third approach is to treat the CWS as a 3D layer of infinitesimal thickness ε . For some $\mathbf{y} \in S$ and if \mathbf{j} is smooth enough, we could compute the $\varepsilon \rightarrow 0$ limit of

$$\tilde{\mathbf{L}}_\varepsilon(\mathbf{j}_\varepsilon)(\mathbf{y}) = \int_{-\varepsilon/2}^{\varepsilon/2} [\mathbf{j}_\varepsilon(\mathbf{y} + \varepsilon_1 \mathbf{n}(\mathbf{y})) \times \mathbf{B}(\mathbf{y} + \varepsilon_1 \mathbf{n}(\mathbf{y}))] d\varepsilon_1.$$

Note that $\mathbf{B}(\mathbf{y} + \varepsilon_1 \mathbf{n}(\mathbf{y}))$ is well-defined as we integrate on a 3D domain, and is given by:

$$\mathbf{B}(\mathbf{y} + \varepsilon_1 \mathbf{n}(\mathbf{y})) = \int_S \int_{-\varepsilon/2}^{\varepsilon/2} [\mathbf{j}_\varepsilon(\mathbf{x} + \varepsilon_2 \mathbf{n}(\mathbf{x})) \times \frac{\mathbf{y} - \mathbf{x} + \varepsilon_1 \mathbf{n}(\mathbf{y}) - \varepsilon_2 \mathbf{n}(\mathbf{x})}{|\mathbf{y} - \mathbf{x} + \varepsilon_1 \mathbf{n}(\mathbf{y}) - \varepsilon_2 \mathbf{n}(\mathbf{x})|^3}] dS(\mathbf{x}) d\varepsilon_2.$$

In order to approximate the 3D volume with a 2D current-sheet, we suppose that $\forall z \in S$ and $\forall \varepsilon'$, it is $\mathbf{j}_\varepsilon(\mathbf{z} + \varepsilon' \mathbf{n}(\mathbf{z})) = \frac{\mathbf{j}(\mathbf{z})}{\varepsilon}$. Thus,

$$\tilde{\mathbf{L}}_\varepsilon(\mathbf{j}_\varepsilon) = \frac{1}{\varepsilon^2} \int_{-\varepsilon/2}^{\varepsilon/2} \int_{-\varepsilon/2}^{\varepsilon/2} \left\{ \int_S \mathbf{j}(\mathbf{y}) \times \left[\mathbf{j}(\mathbf{x}) \times \frac{\mathbf{y} - \mathbf{x} + \varepsilon_1 \mathbf{n}(\mathbf{y}) - \varepsilon_2 \mathbf{n}(\mathbf{x})}{|\mathbf{y} - \mathbf{x} + \varepsilon_1 \mathbf{n}(\mathbf{y}) - \varepsilon_2 \mathbf{n}(\mathbf{x})|^3} \right] dS(\mathbf{x}) \right\} d\varepsilon_2 d\varepsilon_1$$

The quantity inside the brackets is very close to the one we got in Theorem 1, starting with Eqs. 1 and 2, except that we also have a contribution from $\varepsilon_2 \mathbf{n}(\mathbf{x})$. It is possible to prove, using an argument similar to Lemma 5, that replacing $\mathbf{n}(\mathbf{x})$ with $\mathbf{n}(\mathbf{y})$ does not change the limit. The intuition is that for \mathbf{x} close to \mathbf{y} , $\mathbf{n}(\mathbf{x})$ is close to $\mathbf{n}(\mathbf{y})$. As a result, $\tilde{\mathbf{L}}_\varepsilon(\mathbf{j})$ has the same limit as $\mathbf{L}_\varepsilon(\mathbf{j})$ and the expression we found for the Laplace force (Eqs. 4-7) is consistent.

3 Examples of cost functions

After having rigorously defined the Laplace force-density $\mathbf{L}(\mathbf{j})(\mathbf{y})$ that a current-sheet of density \mathbf{j} exerts on itself at location y (Eqs. 4-7 for $\mathbf{j}_1 = \mathbf{j}_2 = \mathbf{j}$), we now introduce some cost-functions to penalize high values of the force.

Two main options are possible, and considered here: (1) penalizing high cumulative (or, equivalently, surface-averaged) forces, or (2) penalizing or even forbidding excessively high local maxima of the force. Further variants are possible for specific force-components (e.g. tangential or normal to the CWS) or a weighted combination of them, with higher weights assigned to the engineeringly more demanding component, depending on the specific stellarator design. Such variants go beyond the scope of the present paper, and are left for future work.

A natural choice from the functional analysis point of view is to use a penalization of the form

$$|\mathbf{L}(\mathbf{j})|_{L^p(S, \mathbb{R}^3)} = \left(\int_S |\mathbf{L}(\mathbf{j})(\mathbf{x})|^p d\mathbf{x} \right)^{1/p}. \quad (30)$$

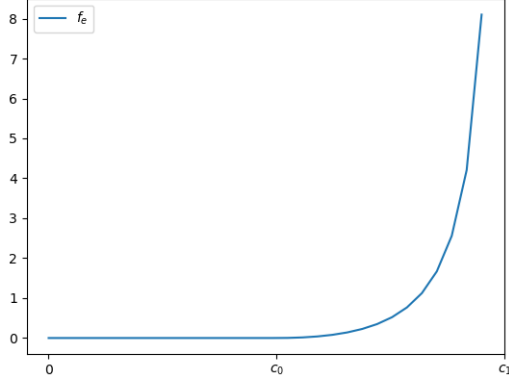


Figure 2: Plot of the local cost f_e as a function of the local force w . Note that f_e diverges at c_1 and vanishes in $[0, c_0]$.

The case $p = 2$ is well-known: it represents the cumulative (or, barring a factor, the surface-averaged) root-mean-square force. Higher values of p penalize more severely high values of the Laplace force (i.e., large oscillations around the average norm). By contrast, low values of p penalize the average norm of the Laplace force.

In principle it is also possible to use a L^∞ cost, $\sup_S |\mathbf{L}(\mathbf{j})|$, but the domain might be smaller than $\mathfrak{X}^{1,2}(S)$. However, such cost is not differentiable whenever the maximum is reached at multiple locations.

The second option is to introduce the cost

$$C_e(j) = \int_S f_e(\mathbf{L}(\mathbf{j})(\mathbf{x})) d\mathbf{x} \quad (31)$$

as the surface integral of the local cost

$$f_e(w) = \frac{\max(w - c_0, 0)^2}{1 - \frac{\max(w - c_0, 0)}{c_1 - c_0}}. \quad (32)$$

The domain for this cost is not the entire space $\mathfrak{X}^{1,2}(S)$, but this cost captures more effectively the engineering constraints of building a high-field stellarator: the mechanical properties of support-structures and materials are such that forces below a threshold c_0 are negligible, forces higher and higher than c_0 should be penalized more and more, and forces above a second, “rupture”

threshold c_1 should be completely forbidden. Indeed, the local cost f_e evolves with the local force w as desired, as illustrated in Figure 2.

Remark 4. *It is unclear whether a minimizer exists in $\mathfrak{X}^{1,2}(S)$ for the costs discussed. As a consequence, a good practice is to add a regularizing term $|\mathbf{j}|_{\mathfrak{X}^{1,2}(S)}$.*

4 Numerical simulations

4.1 Setup

To test our force-reduction method, we ran simulations for the NCSX stellarator equilibrium known as LI383 [20].

As mentioned in the Introduction, the costs defined in Sec. 3 are easily added to the cost-function in any stellarator coil optimization code. In our case such code was a new incarnation of REGCOIL, which we rewrote in python instead of fortran, and compiled with the Just In Time compiler Numba [21]. For the most part the new code is conceptually identical to REGCOIL, except that it uses Eq. A5 of Ref. [1] in lieu of its normal, single-valued component (Eq. A8 from the same paper). Eq. A5 would be numerically unstable if derivatives were taken by finite differences, but can be used here because we compute the derivatives explicitly. We benchmarked the new code and found it to agree with the original REGCOIL to within 7 significant digits.

The surface-current \mathbf{j} is divergence-free and thus taken in the form

$$G \frac{\partial \mathbf{r}'}{\partial \theta} - I \frac{\partial \mathbf{r}'}{\partial \zeta} + \frac{\partial \Phi'}{\partial \zeta'} \frac{\partial \mathbf{r}'}{\partial \theta'} - \frac{\partial \mathbf{r}'}{\partial \zeta'} \frac{\partial \Phi'}{\partial \theta'}. \quad (33)$$

Here θ and ζ are the poloidal and toroidal angle, G and I are optimization inputs (net poloidal and toroidal currents) and the current potential Φ is decomposed in a 2D Fourier basis.

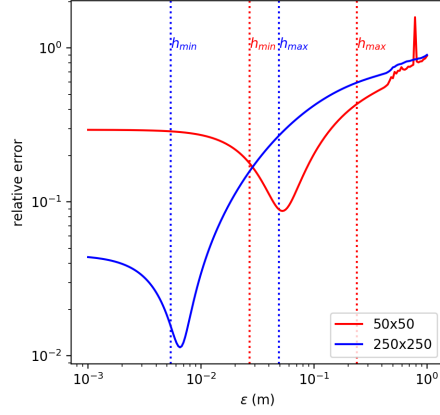


Figure 3: Convergence of \mathbf{L}_ε toward \mathbf{L} for NCSX, for two different grids. Convergence stops when $\varepsilon \lesssim h$, due to a numerical error in \mathbf{B} (Figure 1).

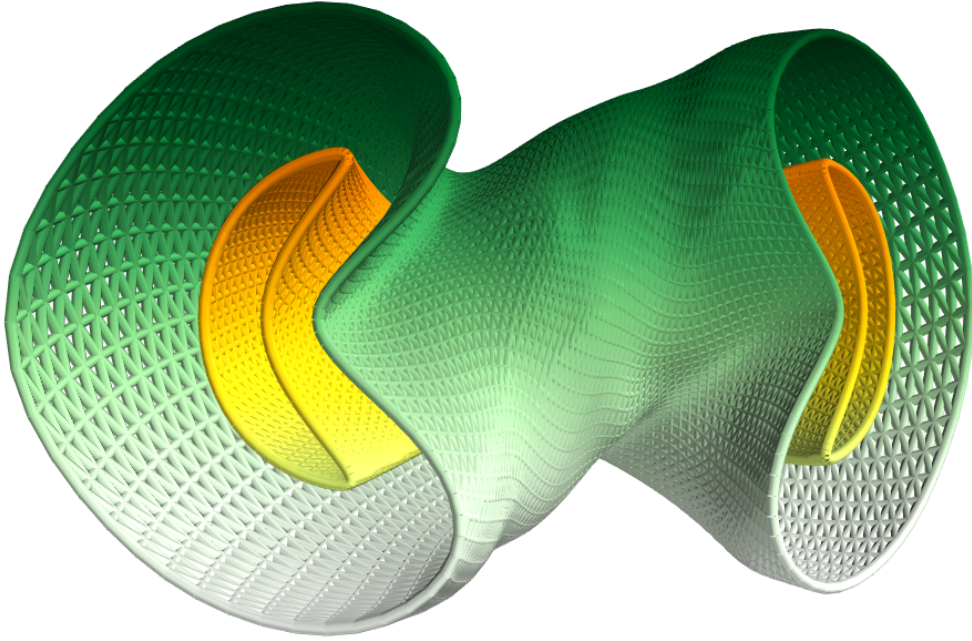


Figure 4: NCSX LI383 plasma surface in orange and CWS in green.

Figure 3 illustrates how \mathbf{L}_ε converges to \mathbf{L} (or, equivalently, the relative error vanishes) as $\varepsilon \rightarrow 0$. We recall that the numerical evaluation of \mathbf{L}_ε involves

three characteristic distances h (discretisation length of the mesh), ε , and d_B (characteristic distance of variation of the magnetic field). For reference we computed \mathbf{L} on the same mesh (that is, for the same h), and obviously d_B was also the same.

We observe that the error decreases with ε , as expected, but when $\varepsilon \lesssim h$ the convergence stops and the error grows again. This is a consequence of the calculation of \mathbf{B} not being accurate anymore, for $\varepsilon \lesssim h$ (see Figure 1). Note that the reference value itself is an approximation. As we do not have an analytic expression, we also used a discretisation. The relative error is computed in L^2 norm.

In all simulations presented here, both the CWS and the plasma surface were discretized as 64×64 meshes in the poloidal \times toroidal direction. The two surfaces are rendered in 3D in Figure 4.

The single-valued current potential Φ from which \mathbf{j} descends is represented by 8 or 12 harmonics in each direction. As we do not impose stellarator symmetry, we use as a basis the functions

$$\sin(k\theta + l\zeta), \quad \cos(k\theta + l\zeta)$$

with $0 \leq k \leq N$ and $-N \leq l \leq N$. Since for $k = 0$ we can restrict to $0 < l$, the total number of Degrees Of Freedom (DOF) is $2[(2N + 1)N + N]$.

Thus $N = 8$ harmonics in each direction correspond to 288 DOF, and $N = 12$ yields 624 DOF. Better results can be achieved with more harmonics, as shown in Figure 5. However, a finer mesh is required, making the problem computationally more expensive.

The optimization is performed by conjugate gradient. With our implementation, a single evaluation of the gradient lasts approximately 2 minutes on a small cluster of 64 cores. The full optimization can last a few days.

4.2 Adding force minimization and improving regularization in REGCOIL

We propose to integrate the costs introduced above in the same optimization scheme as NESCOIL [15] and REGCOIL [1].

As a reminder, NESCOIL seeks the current of density \mathbf{j} , on a fixed S , that maximizes magnetic field accuracy on the plasma boundary S_P (hence, indirectly, in the plasma). It does so by minimizing the “plasma-shape objective”

or “field accuracy objective”

$$\chi_B^2 = \int_{S_P} \langle \mathbf{B}(\mathbf{x}) \cdot \mathbf{n}(\mathbf{x}) \rangle^2 dS(\mathbf{x}). \quad (34)$$

REGOIL, instead, compromises between field accuracy and coil simplicity by minimizing $\chi_B^2 + \lambda \chi_j^2$, where λ is a weight and the “current-density objective” or “regularizing term” χ_j^2 is a penalty on high values of \mathbf{j} , in the sense of the L^2 norm:

$$\chi_j^2 = \int_S |\mathbf{j}|^2 dS. \quad (35)$$

Heavier weighting makes Φ (hence \mathbf{j} , hence the coils) more regular, but at the expense of reduced field accuracy. Such cost is identical to χ_K^2 of Ref. [1], but is renamed χ_j^2 for consistency of notation with another regularizing term that we need to introduce:

$$\chi_{\nabla \mathbf{j}}^2 = \int_S (|\nabla \mathbf{j}_x|^2 + |\nabla \mathbf{j}_y|^2 + |\nabla \mathbf{j}_z|^2) dS. \quad (36)$$

This new term is motivated by Theorem 1: as the Laplace force can only be defined for $\mathbf{j} \in \mathfrak{X}^{1,2}(S)$, it is natural to add a penalization on the gradient of \mathbf{j} and not just on \mathbf{j} . Basically we are replacing the L^2 norm of \mathbf{j} with the H^1 norm of \mathbf{j} .

Here we propose to further generalize the REGCOIL cost function to

$$\chi^2 = \chi_B^2 + \lambda_1 \chi_j^2 + \lambda_2 \chi_{\nabla \mathbf{j}}^2 + \gamma \chi_F^2, \quad (37)$$

where χ_F^2 is a “force objective” that penalizes strong forces on the current-sheet, i.e. among the coils. Per the discussion in Sec. 3, possible definitions include:

$$\chi_F^2 = |\mathbf{L}(\mathbf{j})|_{L^2(S, \mathbb{R}^3)}^2 = \int_S |\mathbf{L}(\mathbf{j})|^2 dS \quad (38)$$

$$\chi_F^2 = C_e = \int_S f_e(|\mathbf{L}(\mathbf{j})|) dS \quad (39)$$

with f_e defined as in Eq. 32 and plotted in Fig. 2. As stress limits, here we set $c_0 = 5 \cdot 10^6$ Pa and $c_1 = 10^7$ Pa.

4.3 Numerical results

There is obviously a trade-off between conflicting objectives in Eq. 37. To study that, we compared a REGCOIL-like case with a force-minimization case.

In the REGCOIL-like case (curves in Fig. 5) we fixed $\lambda_2 = \gamma = 0$ and minimized $\chi^2 = \chi_B^2 + \lambda_1 \chi_j^2$ for various choices of λ_1 . By this scan we re-obtained the well-known trade-off between χ_B^2 and χ_j^2 (or, equivalently, field-accuracy and coil-simplicity) exhibited by REGCOIL [1] (not plotted). Interestingly, we also found a trade-off between χ_B^2 and χ_F^2 , even though χ_F^2 was not part of the $\chi_B^2 + \lambda_1 \chi_j^2$ minimization. The trade-off between these global quantities is plotted in Fig. 5a, and a trade-off between related, local quantities is plotted in Fig. 5b. In other words, more (less) accurate solutions tend to be subject to higher (lower) forces, even when forces are not accounted in the minimization.

In the force-minimization case, instead, we fixed $\lambda_1 = \lambda_2 = 0$ and minimized $\chi^2 = \chi_B^2 + \gamma \chi_F^2$ for various choices of γ . Not surprisingly, we found a trade-off between χ_B^2 and χ_F^2 (symbols in Fig. 5). Interestingly, we also found a trade-off between χ_B^2 and χ_j^2 , even though χ_j^2 was not part of the minimized cost. This suggests that χ_F has a regularizing effect on \mathbf{j} , as it will become apparent in Fig. 7 and 8.

Finally, Fig. 5 confirms that a higher number of Fourier harmonics and hence of DOF reproduces the magnetic field more accurately. This is why for the remainder of the article we adopt the higher number of DOF, 624.

Also, we no longer scan the weights, but fix them to yield reasonable compromises between field accuracy, current regularization and/or force minimization. In particular, calculations were performed for the following four choices of weights and χ_F in Eq. 37:

Case	λ_1 (T ² m ² /A ²)	λ_2 (T ² m ⁴ /A ²)	γ (T ² /Pa ²)	χ_F	(40)
1	$1.5 \cdot 10^{-16}$	0	0	0	
2	0	0	10^{-17}	$ \mathbf{L}(\mathbf{j}) _{L^2(S, \mathbb{R}^3)}^2$	
3	0	0	10^{-16}	C_e	
4	10^{-19}	10^{-19}	10^{-16}	C_e	

Case 1 is basically REGCOIL, whereas case 2 and 3 are effectively NESCOIL but with minimized forces, according to two different force metrics. Finally,

case 4 explicitly combines force minimization with regularization, but in a broader sense compared to REGCOIL, as discussed in connection with Eq. 36.

The results for these four cases are plotted in Fig. 6 (circles) and compared with REGCOIL results (curve). In particular Fig. 6a refers to surface-integrated, “global” objectives, and Fig. 6b to “local” maxima. Note the logarithmic plots. As expected, case 1 agrees with REGCOIL. Case 2 (defined in terms of the “global” $|\mathbf{L}(\mathbf{j})|_{\mathcal{E}_2}^2$) overperforms in the “global” Fig. 6a, as expected. Actually, it performs better than REGCOIL even in terms of local metrics (Fig. 6b). Compared to REGCOIL, peak-forces are reduced in cases 3 and 4 (Fig. 6b), and remain lower than the chosen c_1 , as is expected from the definition of C_e and f_e (Eqs. 31-32) However, this happens at the expense of higher cumulative forces (Fig. 6a).

Details on the four cases are presented in Fig. 7 and 8. Columns from left to right refer to cases from 1 to 4. From top to bottom, the rows in Fig. 7 present contours of the norm of \mathbf{j} , the component of the magnetic field normal to S and the norm of the Laplace force, as functions of the poloidal and toroidal angles. The two rows in Fig. 8 present the force components normal and tangential to S .

As anticipated, case 2 is as regular as case 1, in spite of its χ^2 not containing a regularizing objective. By contrast, case 3 reproduces the field with high accuracy and exhibits reduced peak forces, as expected from the definition of C_e , but with a complicated current-pattern. That is ameliorated by adding some regularization: case 4 is the best compromise between coil simplicity (first row in Fig. 8), field accuracy (second row) and reduced forces (third row).

Incidentally all cases, including REGCOIL (case 1) and the magnetically most accurate case 3, exhibit residual field errors of up to 60 mT. Lower errors can be achieved by adopting a higher number of DOF, as is intuitive and suggested by Fig. 5, but this is computationally more intensive and beyond the scope of the present paper.

From the point of view of the surface-integrated or surface-averaged forces, the best result in Fig. 7 is a modest reduction by 5% for case 2, relative to REGCOIL. From the point of view of peak forces, however, the best result in Fig. 7 is a reduction by 40% for case 4, relative to REGCOIL. Correspondingly, the peak tangential force is reduced by 50% and the peak normal force by 20% (Fig. 8). Note that maxima for different components occur at different toroidal and poloidal locations.

More dramatic reductions were obtained in Fig. 5, especially in peak

forces. However, they were obtained for low-accuracy cases on the top left of Fig. 5b: a stellarator with those characteristics would suffer from very low coil-forces, but it would also be a poor match of the target field.

5 Summary, conclusions and future work

To summarize, force-minimization is an important aspect of stellarator coil-optimization, especially for future high-field stellarators. In the present article we rigorously proved in Sec. 2.3 that the Laplace force exerted by a surface-current onto one another can be written as in Eqs. 4-7). From that, one can calculate the auto-interaction $\mathbf{L}(\mathbf{j})$ of a current-distribution with itself, and distill that information in a single scalar. Possible metrics were discussed in Sec. 3, and two of them were used for detailed numerical calculations: two possible “force objectives” (Eqs. 38 and 39) were added to the cost function of the well-known REGCOIL code [1]. In addition, the L^2 norm of \mathbf{j} was replaced with the H^1 norm of \mathbf{j} , for reasons explained in Secs. 2.2 and 4.2.

This approach permitted to simultaneously optimize the coils of the NCSX stellarator for high magnetic fidelity, high regularity and low forces, e.g. 40% lower peak forces compared to REGCOIL for similar plasma shape accuracy, slightly higher average current and lower current peak (Figs 5-8).

Force reduction is an important criterion in stellarator optimization, and future high-field designs might benefit from our approach.

In the present work the Coil Winding Surface (CWS) was fixed. Future shape optimization of the CWS, inspired by Ref. [22], is expected to further reduce the coil-forces. Moreover, the constraints c_0 and c_1 on penalized and forbidden forces (Fig. 2) were fixed. Future work could impose stricter constraints and tailor them differently for normal and longitudinal forces, as they tend to differ (Fig. 8) and obey to different engineering and material constraints. Finally, the new code is magnetically as accurate as REGCOIL, when operated with the same number of Fourier harmonics and hence of degrees of freedom (DOF). However, it is also significantly slower as a result of force minimization. Optimizing the code for speed would allow to retain a higher number of DOF and achieve higher field accuracy for the same amount of cpu time, while at the same time optimizing for simplicity and force reduction.

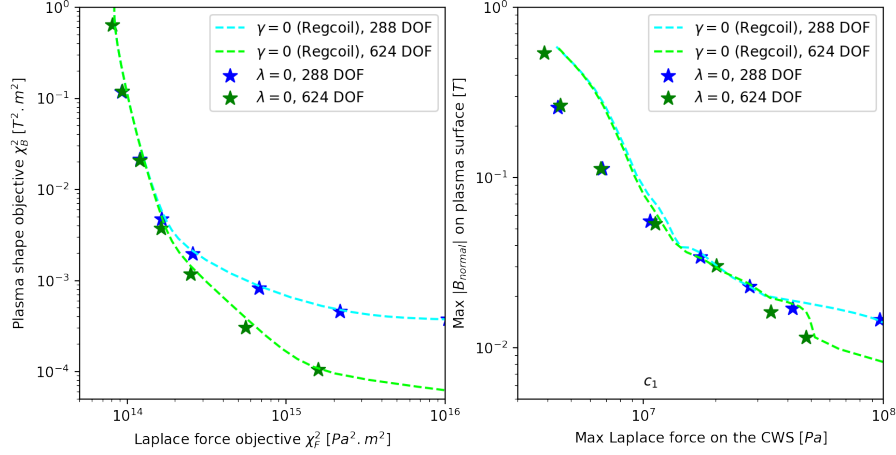


Figure 5: (a) Trade-off between plasma shape accuracy and Laplace force metrics (as defined in Eq. 38) for different weightings in Eq. 37 and different numbers of harmonics, and thus of Degrees of Freedom (DOF). Such trade-off, expected when optimizing a linear combination of χ_B^2 and χ_F^2 (symbols), is also observed in the minimization of χ_B^2 and χ_j^2 (curves). (b) Similar trade-off between maximum field and maximum Laplace force (Eq. 39).

6 Acknowledgements

The authors thank Mario Sigalotti for the fruitful discussions and for carefully reading the manuscript. This work has been partly supported by Inria's Action Exploratoire StellaCage.

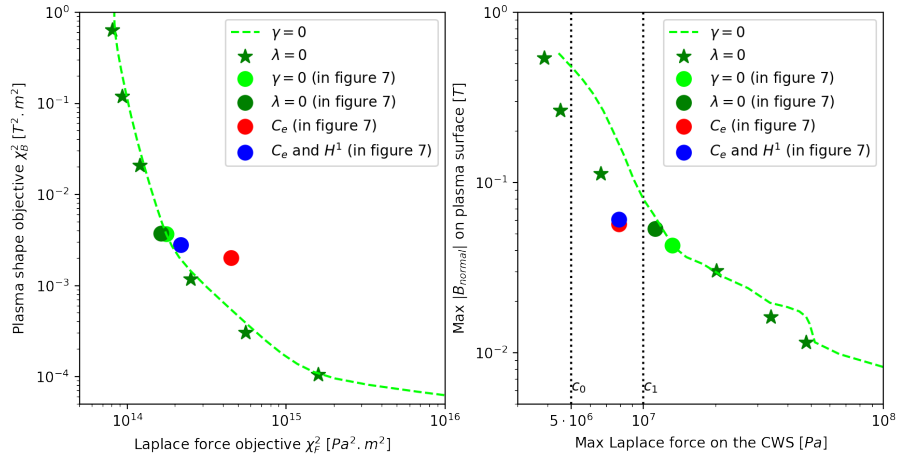


Figure 6: Trade-offs between: (a) plasma shape accuracy and Laplace force metrics (Eq. 38) and (b) maximum field and maximum Laplace force (Eq. 39). Unlike Fig. 5, all simulations here used 624 DOF. Circle symbols correspond to the four cases discussed in Sec. 4 and presented in Figure 7. As expected, the C_e cases (red and blue) fall between the penalized and forbidden forces c_0 and c_1 defined in Fig. 2, marked here by vertical dotted lines.

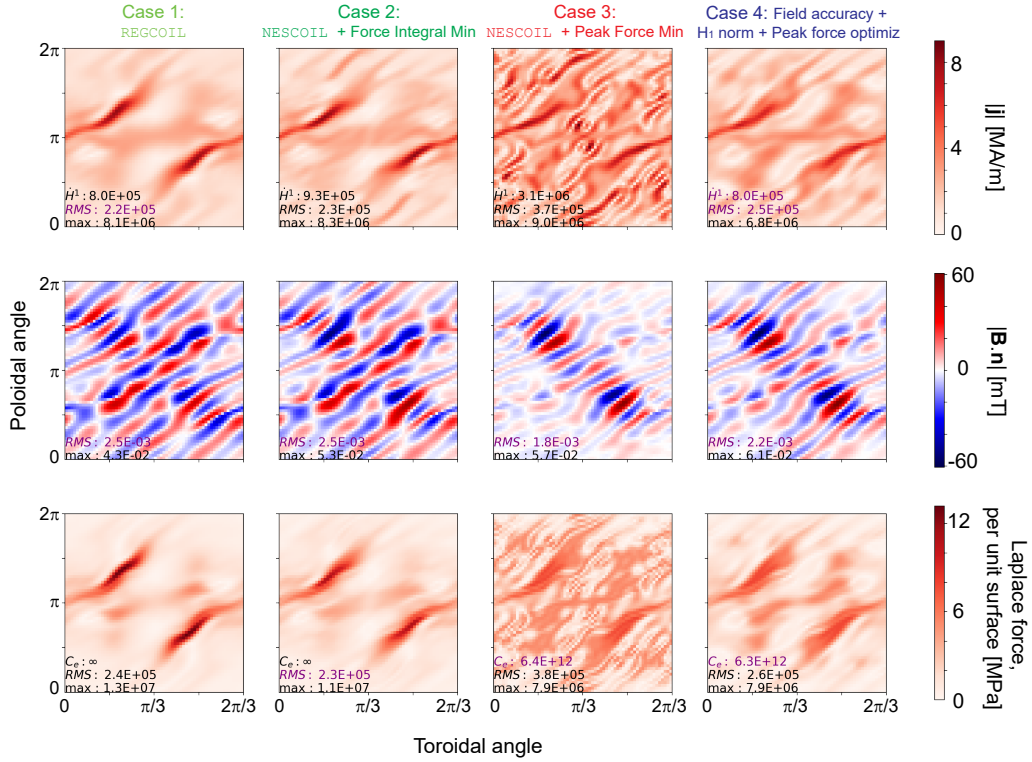


Figure 7: Results of minimizing Eq. 37 for NCSX, for four different weight choices (Eq. 40). 624 DOF are used for \mathbf{j} in every simulation. From top to bottom the three rows refer respectively to the results for simultaneous current regularization (if any), field accuracy and force-minimization (if any). Shown in the legends are the Root Mean Square (RMS) surface-averages and local maxima of the quantities plotted, as well as the H^1 norm of \mathbf{j} and C_e force metric (Eq. 39). The quantities actually minimized are marked in purple.

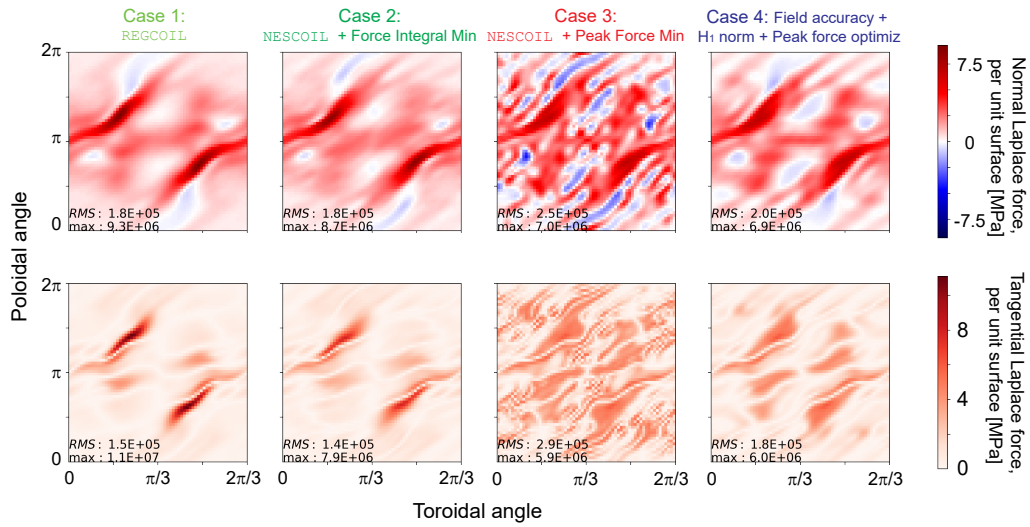


Figure 8: Tangential and normal components of the Laplace forces of the simulations in Figure 7.

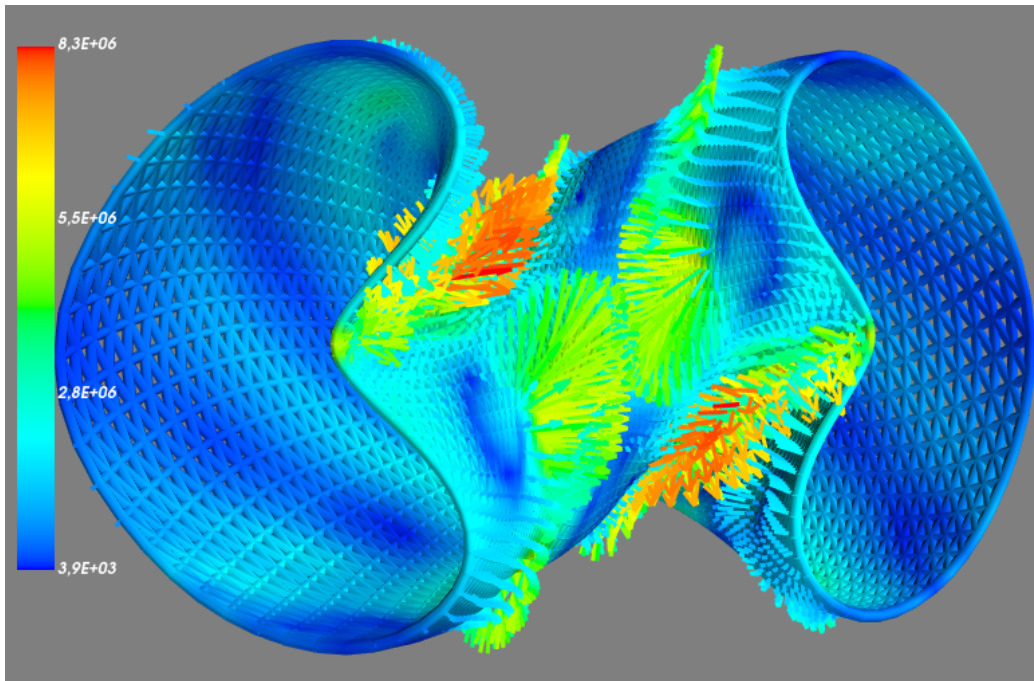


Figure 9: The Laplace forces from the last column of Figure 7. The unit for the pressure is Pascal.

References

- [1] M. Landreman. An improved current potential method for fast computation of stellarator coil shapes. *Nuclear Fusion*, 57(4):046003, April 2017.
- [2] P. Helander. Theory of plasma confinement in non-axisymmetric magnetic fields. *Reports on Progress in Physics*, 77(8):087001, jul 2014.
- [3] E.S. Marmor, S.G. Baek, H. Barnard, P. Bonoli, D. Brunner, J. Candy, et al. Alcator c-mod: research in support of iter and steps beyond. *Nucl. Fusion*, 55:104020, 2015.
- [4] G. Pucella, E. Alessi, L. Amicucci, B. Angelini, M. L. Apicella, G. Apruzzese, G. Artaserse, E. Barbato, F. Belli, et al. Overview of the FTU results. *Nuclear Fusion*, 55(10):104005, October 2015.
- [5] B. Coppi, A. Airoidi, R. Albanese, G. Ambrosino, F. Bombarda, A. Bianchi, A. Cardinali, G. Cenacchi, E. Costa, P. Detragiache, and others. New developments, plasma physics regimes and issues for the Ignitor experiment. *Nuclear Fusion*, 53(10):104013, October 2013.
- [6] D. Meade, S. Jardin, C. Kessel, J. Mandrekas, M. Ulrickson, et al. Fire, exploring the frontiers of burning plasma science. *J. Plasma Fusion Res. SER.*, 5:143148, 2002.
- [7] A. J. Creely, M. J. Greenwald, S. B. Ballinger, D. Brunner, J. Canik, J. Doody, T. Fülöp, D. T. Garnier, R. Granetz, T. K. Gray, and et al. Overview of the SPARC tokamak. *Journal of Plasma Physics*, 86(5):865860502, 2020.
- [8] A. Sagara, Y. Igitkhanov, and F. Najmabadi. Review of stellarator/heliotron design issues towards MFE DEMO. *Fusion Engineering and Design*, 85(7):1336 – 1341, 2010. Proceedings of the Ninth International Symposium on Fusion Nuclear Technology.
- [9] V. Queral, F.A. Volpe, D. Spong, S. Cabrera, and F. Tabarés. Initial exploration of high-field pulsed stellarator approach to ignition experiments. *Journal of Fusion Energy*, 37:275, 2018.
- [10] Type one energy. <https://www.typeoneenergy.com>.

- [11] Renaissance fusion. <https://stellarator.energy>.
- [12] Felix Schauer, Konstantin Egorov, and Victor Bykov. Helias 5-b magnet system structure and maintenance concept. *Fusion Engineering and Design*, 88(9):1619 – 1622, 2013. Proceedings of the 27th Symposium On Fusion Technology (SOFT-27); Liège, Belgium, September 24-28, 2012.
- [13] S. Imagawa, A. Sagara, K. Watanabe, T. Satow, and O. Motojima. Magnetic field and force of helical coils for force free helical reactor (ffhr). *J. Plasma Fusion Res. SERIES*, 5:537, 2002.
- [14] A. Alonso-Rodríguez, J. Camanõ, R. Rodríguez, , A. Valli, and P. Venegas. Finite element approximation of the spectrum of the curl operator in a multiply connected domain. *Found. Comput. Math*, 1:1493, 2018.
- [15] P. Merkel. Solution of stellarator boundary value problems with external currents. *Nuclear Fusion*, 27(5):867–871, May 1987. Publisher: IOP Publishing.
- [16] Dennis Strickler, S. Hirshman, D. Spong, Mpilo Cole, James Lyon, B. Nelson, David Williamson, and Andrew Ware. Development of a Robust Quasi-Poloidal Compact Stellarator. *Fusion Science and Technology*, 45:15–26, January 2004.
- [17] Caoxiang Zhu, Stuart R. Hudson, Yuntao Song, and Yuanxi Wan. New method to design stellarator coils without the winding surface. *Nuclear Fusion*, 58(1):016008, January 2018. arXiv: 1705.02333.
- [18] Yazhou Han and Meijun Zhu. Hardy-Littlewood-Sobolev inequalities on compact Riemannian manifolds and applications. *Journal of Differential Equations*, 260(1):1–25, January 2016.
- [19] E. Hebey. *Nonlinear Analysis on Manifolds: Sobolev Spaces and Inequalities: Sobolev Spaces and Inequalities*. Courant lecture notes in mathematics. Courant Institute of Mathematical Sciences, 2000.
- [20] M C Zarnstorff, L A Berry, A Brooks, E Fredrickson, G-Y Fu, S Hirshman, S Hudson, L-P Ku, E Lazarus, D Mikkelsen, D Monticello, G H Neilson, N Pomphrey, A Reiman, D Spong, D Strickler, A Boozer, W A Cooper, R Goldston, R Hatcher, M Isaev, C Kessel, J Lewandowski,

- J F Lyon, P Merkel, H Mynick, B E Nelson, C Nuehrenberg, M Redi, W Reiersen, P Rutherford, R Sanchez, J Schmidt, and R B White. Physics of the compact advanced stellarator NCSX. *Plasma Phys. Control. Fusion*, 43(12A):A237–A249, nov 2001.
- [21] Siu Kwan Lam, Antoine Pitrou, and Stanley Seibert. Numba: A llvm-based python jit compiler. In *Proceedings of the Second Workshop on the LLVM Compiler Infrastructure in HPC*, LLVM '15, New York, NY, USA, 2015. Association for Computing Machinery.
- [22] Elizabeth Paul. Adjoint methods for stellarator shape optimization and sensitivity analysis, 2020.